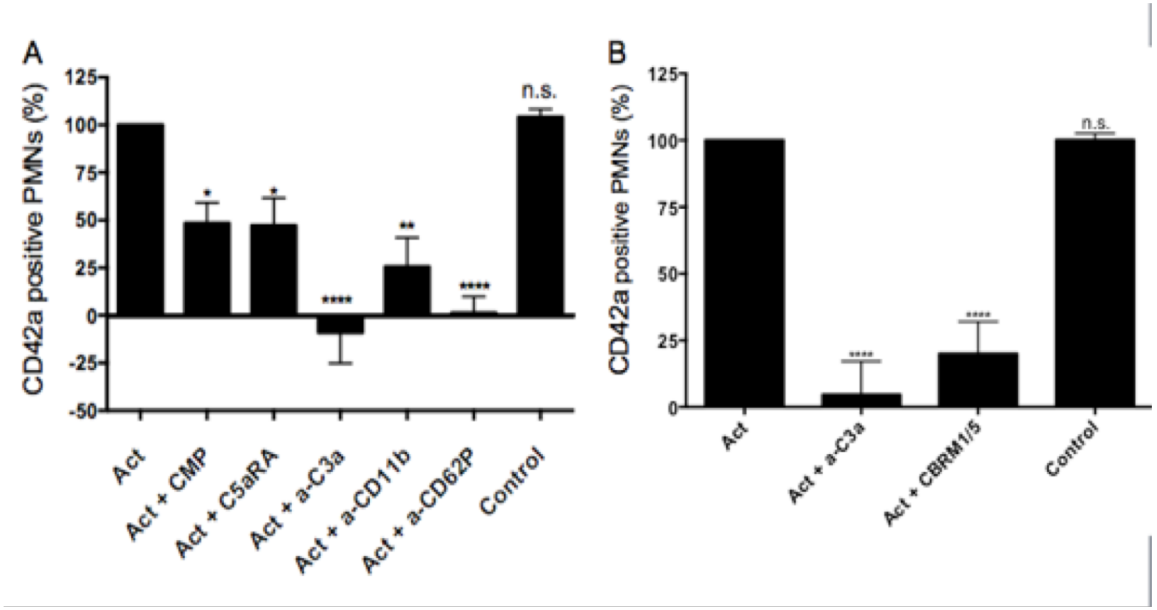

Fig 1: Formation of PMN ($CD16^+$)-platelet ($CD42a^+$) complexes in whole blood after activation (Act) with 33.5 µM TRAP-6, as assessed by flow cytometry (A). Anti-CD11b and anti-C3a inhibited conjugate formation (B).

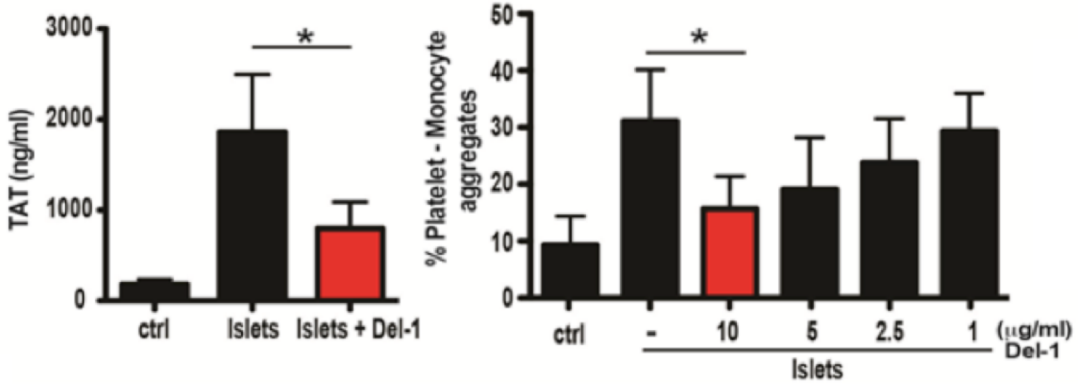

Fig. 2 Del-1 attenuated thrombin-antithrombin (TAT) complex generation and platelet-monocyte aggregation in human whole blood incubated onto porcine islets of Langerhans.

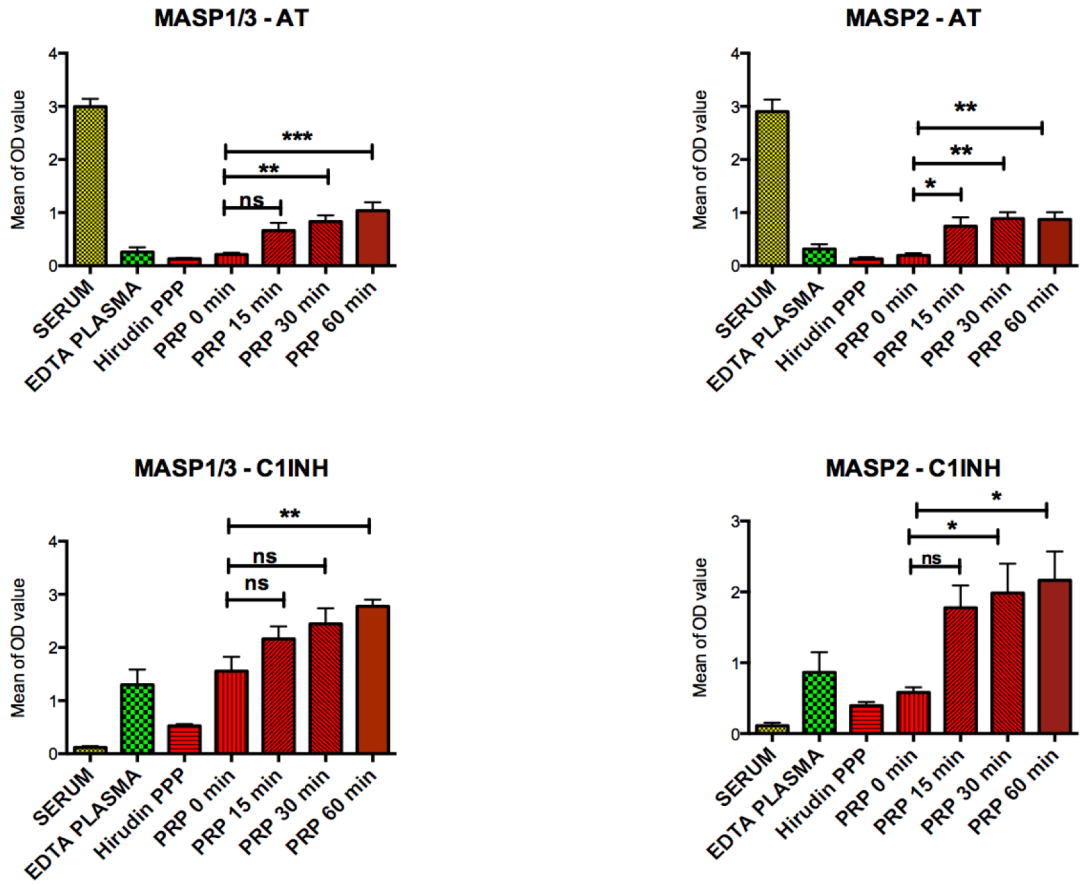

Fig. 3 Panels A–D: formation of MASP-1/C1-INH, MASP-2/C1-INH, MASP-1/AT and MASP-2/AT complexes in serum, EDTA-PPP, lepirudin-PPP and the supernatants of TRAP6-activated lepuridin-PRP from five different donors incubated for 0, 15, 30 or 60 min at 37 °C (*P < 0.05, **P < 0.01, ***P < 0.001). Samples of PPP contained low levels of MASP-1/AT and MASP-2/AT complexes and moderate levels of MASP-1/C1-INH and MASP-2/C1-INH complexes, while the opposite relationship was seen in serum. Activation of PRP induced a time dependent formation of both the MASP-1/C1-INH and MASP-2/C1-INH, and MASP-1/AT and MASP-2/AT, complexes. Panels E–G: formation of MASP complexes detected by SDS-PAGE followed by Western blotting. The complexes were pulled out of serum or plasma obtained from TRAP6-activated PRP using magnetic beads coated with either anti-MASP-1 or anti MASP-2.

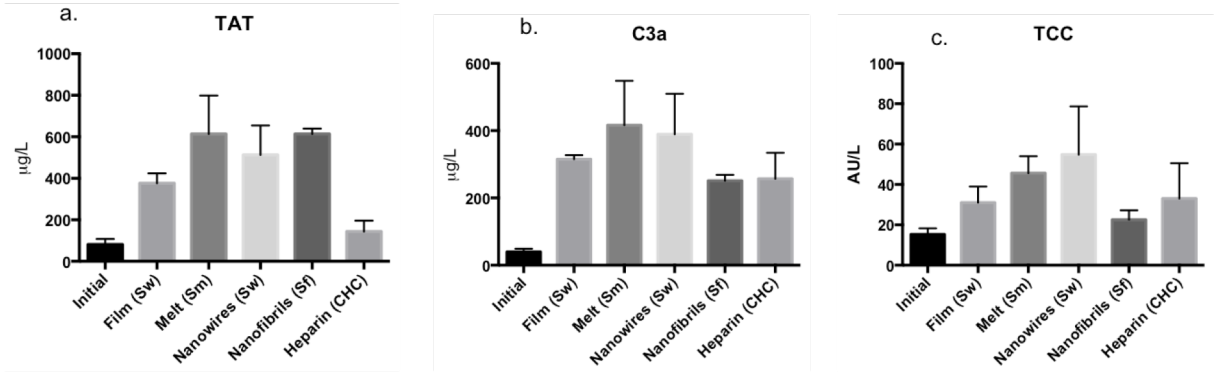

Fig. 4 Results from the TAT (a), C3a (b.) and TCC (c.) ELISAs after the blood chamber experiments using the nanostructures prepared in Task 3b.

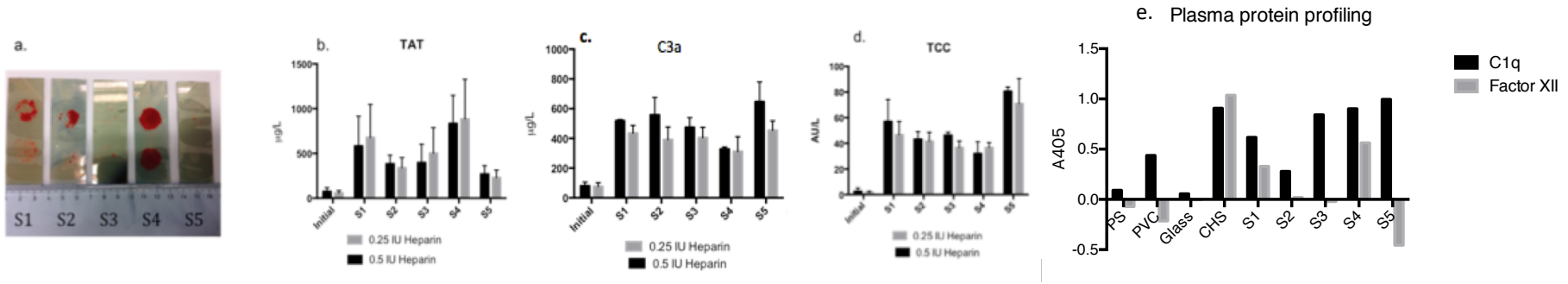

Fig 5 a. Image of the clot formation at the surfaces S1-S5 after incubation in whole blood. b. Result of the TAT ELISA. c. Result from the C3a ELISA. d. Result from the TCC ELISA. e. FXII + C1q

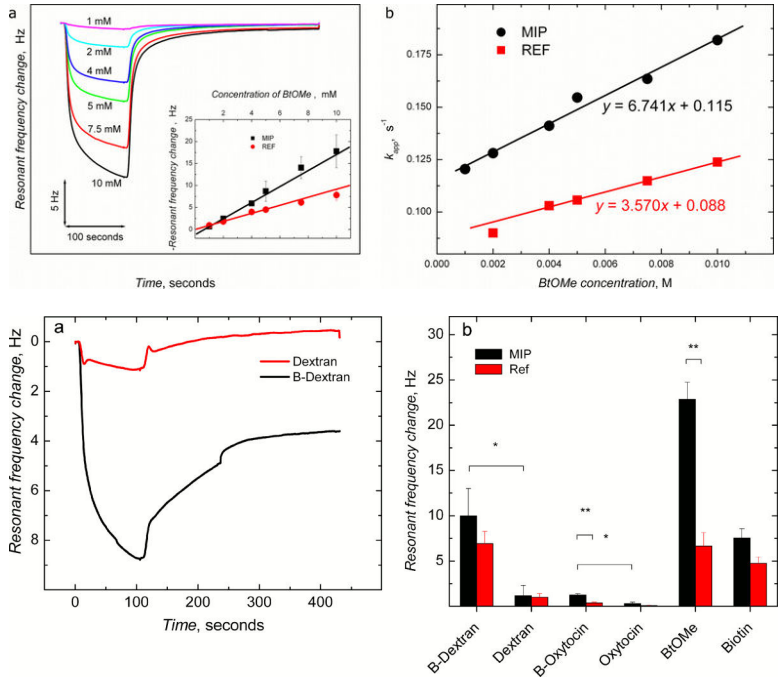

Fig 6 a and b (upper)
Sensitivity and kinetics of polymer-ligand recognition.
(a) Resonant frequency change as a function of BtOMe concentration. Inset is the calibration plot for BtOMe on the MIP (n = 3, 6 injections per surface) and REF (n = 1, 6 injections) films. **(b)** Variation of observed k_{app} calculated from the associative part of the frequency vs time response curves for BtOMe binding to MIP and REF films.
Fig 6 a and b (lower)
Selectivity of polymer-ligand recognition. (a) Frequency response for dextran and biotinylated dextran (B-Dextran) binding to the MIP film. **(b)** Resonant frequency changes for the binding of different analytes to MIP and REF films. * $p > 0.05$, ** $p < 0.01$, n = 3-8, 3–6 injections per surface.

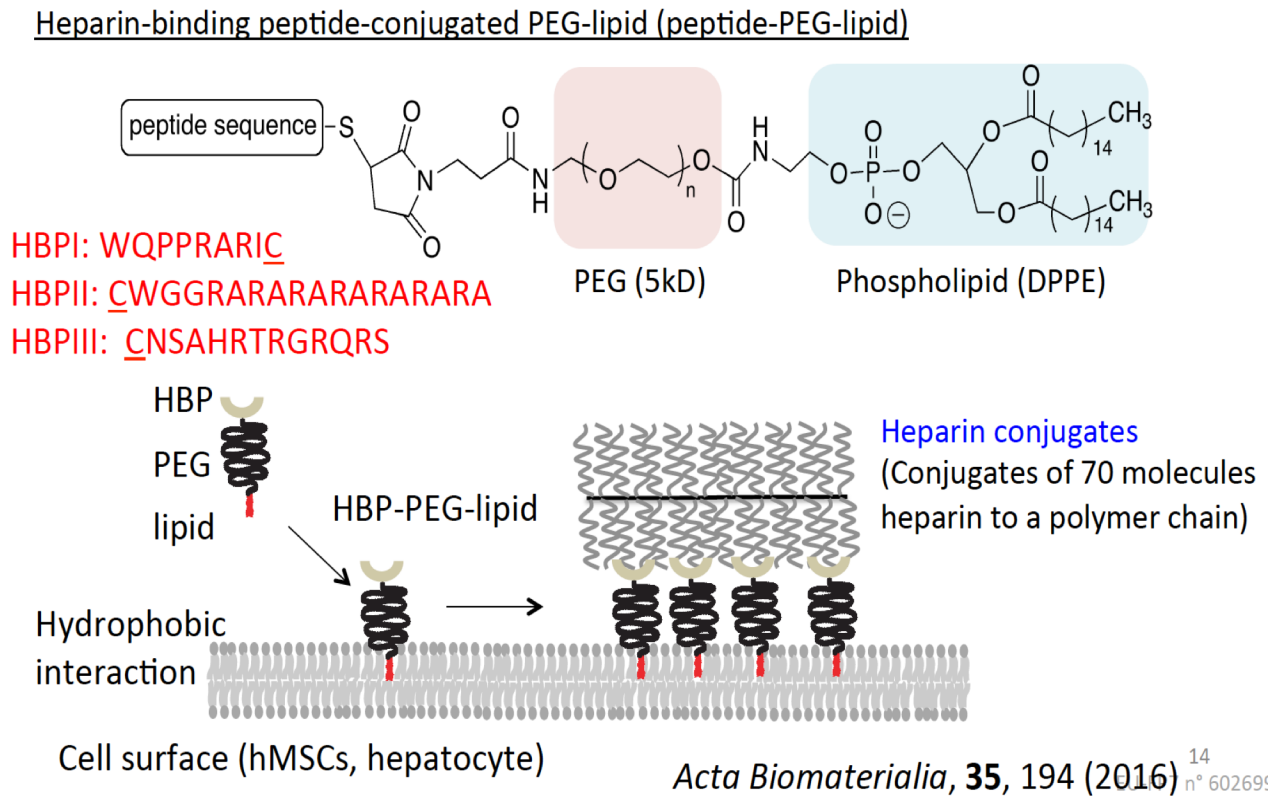

Fig. 7 Surface modification of cell-surface-binding heparin conjugates. Top: chemical structure of heparin-binding peptide-conjugated PEG-lipid for surface modification of cells, and amino acid sequences of heparin-binding peptides either derived from fibronectin (I); positively charged (II); identified by phage display . Bottom: chematic representation of heparin-conjugate immobilization by a cell-surface modification with heparin-binding peptide-PEG-lipid. Each heparin conjugate consisted of a conjugate of approximately 70 heparin molecules to a polymer chain.

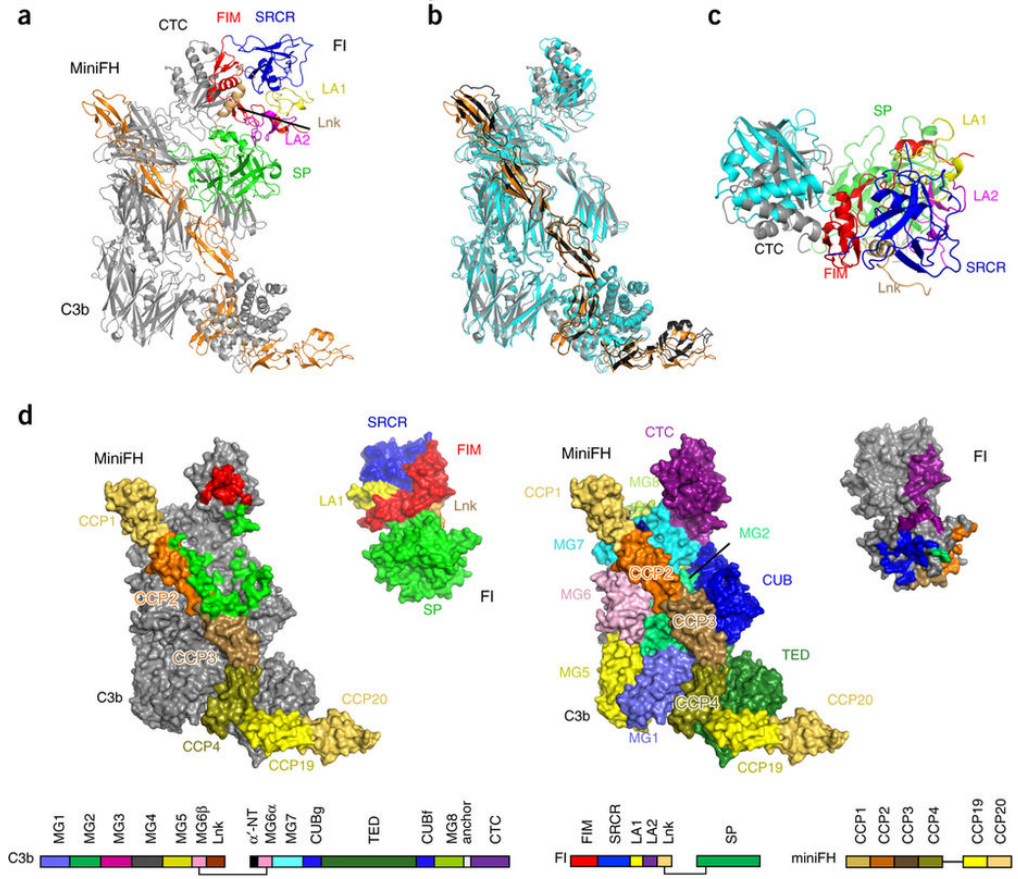

Fig. 8 (**a**) Structure of C3b–miniFH-FI. C3b, gray; miniFH, orange; FI colored by domain as shown at the bottom of the figure. (**b**) Superposition of C3b–miniFH (C3b, cyan; miniFH, black) and the corresponding parts from the C3b–miniFH–FI complex (C3b, gray; miniFH, orange). (**c**) Top view of superposition showing binding of FI (colored by domain as indicated) to CTC domain of C3b (gray); the CTC domain as found in C3b–miniFH is shown (cyan) for reference. (**d**) Contact regions for FI domains shown as footprints on C3b–miniFH (left) and contact region of C3b–miniFH domains on FI (right); domain coloring as defined by labels and schematic domain compositions of C3b, FI and miniFH as shown at the bottom.

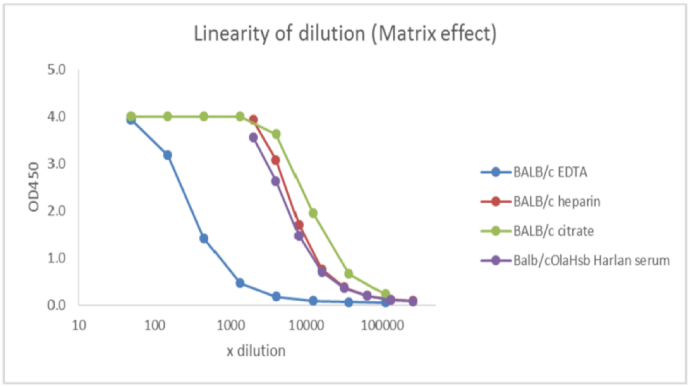

Fig. 9 Detection of mouse C3b-ELISA

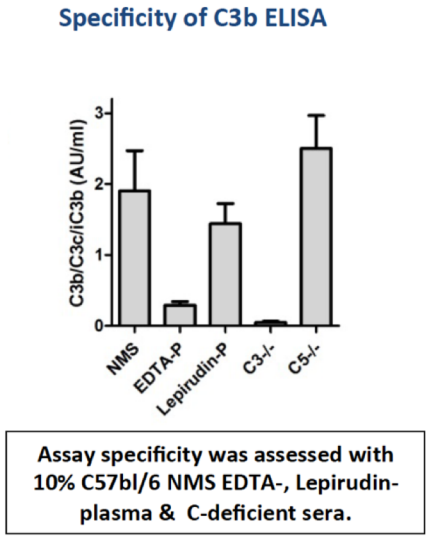

Assay specificity was assessed with 10% C57bl/6 NMS EDTA-, Lepirudin-plasma & C-deficient sera.

Fig. 10 The members of the DIREKT consortium at the Aegean Conference in Chania, Crete, Greece, October 2014.